Supplementary Information for

Hybrid upconversion nanoprobe for ratiometric detection of aliphatic biogenic amines in aqueous medium

Shilpi Jaiswal, Subhankar Kundu, Sujoy Bandyopadhyay[$] and Abhijit Patra*

[$]Present address: Assistant Professor, Department of Chemistry, Indrashil University, Rajpur, Gujarat, India-382740

Department of Chemistry, Indian Institute of Science Education and Research Bhopal (IISERB), Bhopal, India-462066

Fax: +91 (0)755 409 2392; Tel: +91 (0)755 269 1337,

E-mail: abhijit@iiserb.ac.in

Sr. No.	Content	Page. No

I. Instrumentation and chemicals

Steady-state absorption spectroscopy: UV-Visible absorption spectra were recorded on Cary 100 spectrophotometer using 1 cm path length quartz cuvette.

Steady-state fluorescence spectroscopy: Steady-state fluorescence measurements were carried out on a Jobin Yvon Horiba Model Fluoromax Plus spectrofluorometer. A 980 nm continuous wave (CW) laser (4 W) was used as the excitation source for the measurement of upconversion emission.

Time-resolved fluorescence Spectroscopy: The decay measurements were carried out using time-correlated single-photon counting (TCSPC) spectrometer set up (Delta Flex-01-DD/HORIBA). The SpectraLED 461 nm was used as the excitation source. Picosecond photon detection module with photomultiplier tube (PMT) was used as a detector. An aqueous Ludox solution was used to record the instrument response function. Decay curves were analysed by nonlinear least-squares iteration using Horiba EzTime decay analysis software. The quality of the fit was assessed by the fitting parameters (χ^2) and visual inspection of residuals.

Transmission electron microscopy (TEM): Transmission electron microscopy was performed on the FEI TALOS 200S instrument operated at 200 KV.

Powder X-Ray diffraction (PXRD): PXRD measurement was done using a PANalytical Empyrean XRD instrument. Data was collected for 2θ values ranging from 0° to 70°.

Nuclear magnetic resonance (NMR) spectroscopy: ^{1}H NMR spectra were recorded on Bruker Avance III 500 MHz NMR spectrometer, and the chemical shifts (δ) were reported in parts per million (ppm) using residual solvent signals as internal standards.

Matrix-assisted laser desorption ionization (MALDI): Matrix-assisted laser desorption ionization-time of flight mass spectrometry was performed with Bruker Daltonics UltrafleXtreme, using software flex Control version 3.4.

Fourier transform infrared (FTIR) spectroscopy: FTIR measurements were carried out on the Perkin Elmer FTIR spectrophotometer. Ten scans were signal-averaged with a resolution of 4 cm^{-1} at room temperature. KBr pellet was used for the measurements.

Thermogravimetric analysis (TGA): Thermogravimetric analysis was carried out in a Perkin-Elmer (TGA-6000) instrument. The sample was heated at a rate of 10 °C min^{-1} under a nitrogen atmosphere.

Brunauer-Emmett-Teller (BET) specific surface area analysis: All the gas adsorption measurements were performed on Quantachrome Autosorb, QUA211011 equipment. The sample was degassed at 80-100 °C for 12 h under vacuum before analysis. Isotherms were analyzed using ASiQwin software.

Chemicals: Yttrium(III) chloride hexahydrate ($YCl_3 \cdot 6H_2O$, 99.9%), ytterbium(III) chloride hexahydrate ($YbCl_3 \cdot 6H_2O$, 99.9%), thulium(III) chloride hexahydrate ($TmCl_3 \cdot 6H_2O$, 99.9%), ammonium fluoride (NH_4F), oleic acid (OA, 95%), 1-octadecene (ODE, 90%), sodium hydroxide (98%), methanol (99%), tetraethyl orthosilicate (TEOS, 99.9%), cetyltrimethylammonium bromide (CTAB, 98%), ammonium hydroxide solution (NH_4OH, 30%) 4-bromobenzaldehyde, 2,5-thiophenediylbisboronic acid (95%), potassium carbonate (K_2CO_3, 99%), tetrakis(triphenylphosphine)palladium(0) (99%), malononitrile (99%), tetrahydrofuran (THF, 99%), trichloroacetic acid (90%) were received from Sigma-Aldrich and used directly without further purification.

II. Synthesis

2.1 Synthesis of 4,4'-(thiophene-2,5-diyl)dibenzaldehyde (TBA)

TBA was synthesized following a reported procedure with minor modification.[1] 1 eqv. of 2,5-thiophenediylbisboronic acid and 2.5 eqv. of 4-bromobenzaldehyde were taken in a Schleck tube. Then tetrakis(triphenylphosphine)palladium(0) and potassium carbonate were added in the reaction mixture. The mixture was degassed for 5 min and then was kept under an argon atmosphere for 10 min. Further, 10 mL of THF and 1 mL of degassed water were added to the
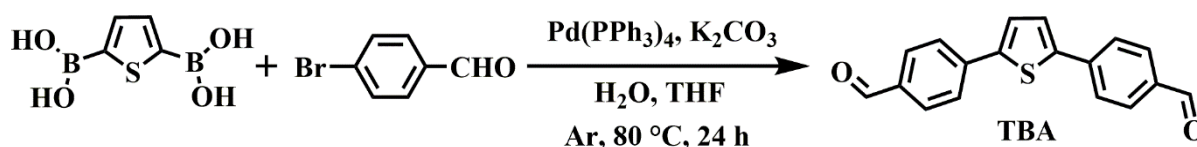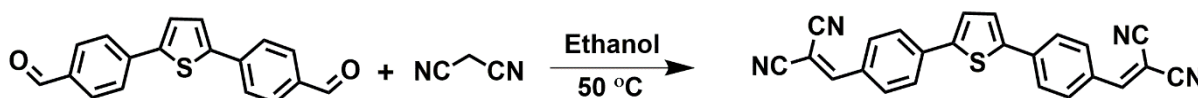

Scheme S1 Synthetic scheme of TBA.

above mixture. The reaction mixture was stirred for 24 h at 80 °C under an argon atmosphere (Scheme S1). Afterward, the reaction mixture was brought to room temperature and washed with ethyl acetate and water multiple times. The organic layer was collected and dried under a vacuum. Further, the product was purified through column chromatography using hexane : EtOAc (4 : 1). A yellow solid product was obtained with 49% yield. The compound was characterized using ^{1}H NMR and mass spectrometry.

^{1}**H NMR** (500 MHz, CDCl$_3$)**:** 10.02 (s, 2H), 7.92 (d, 4H), 7.80 (d, 4H), 7.49 (s, 2H). **MALDI-TOF:** m/z calculated for C$_{18}$H$_{12}$O$_2$S: 292.35 g mol^{-1}; found: 292.66 g mol^{-1} [M$^+$]. **Melting point:** 240 °C.

2.2 Synthesis of 2,2'-((thiophene-2,5-diylbis(4,1-phenylene))bis(methaneylylidene)) dimalononitrile (TDPM)

In a typical reaction procedure, 1 eqv. of TBA and 2.5 eqv. of malononitrile was taken in the Schlenk tube, and ethanol was added to it.[2] The reaction was carried out for 24 h at 50 °C under reflux condition (Scheme S2). The product was collected and washed with hexane multiple times. The product was purified through column chromatography using hexane : EtOAc (9 : 1). A dark red product was obtained with 62% yield.

^{1}**H NMR** (500 MHz, DMSO-d$_6$) δ 8.43 (s, 2H), 7.96 (m, 8H), 7.86 (s, 2H). **MALDI-TOF:** m/z calculated for C$_{24}$H$_{12}$N$_4$S: 388.08 g mol^{-1}; found: 388.03 g mol^{-1} [M$^+$]. **Melting point:** 260 °C.

Scheme S2 Synthetic scheme of TDPM.

III. Characterization

3.1 Transmission electron microscopy (TEM)

Samples for TEM were prepared by dispersing 1 mg of nanoprobes in 3 mL of ethanol and then by drop-casting 10 µL of the dispersion on a carbon-coated 400 mesh Cu grid. The samples were dried for 24 h in a vacuum before taking the images. The TEM images of UCNP, UCNP@mSiO$_2$, and UCNP@mSiO$_2$@TDPM are shown in Fig. S1. The fringes observed in high-resolution transmission electron microscopy (HRTEM) image and selected area electron diffraction (SAED) patterns of UCNP nanocrystals confirmed the crystalline nature of the nanocrystals (Fig. S2).
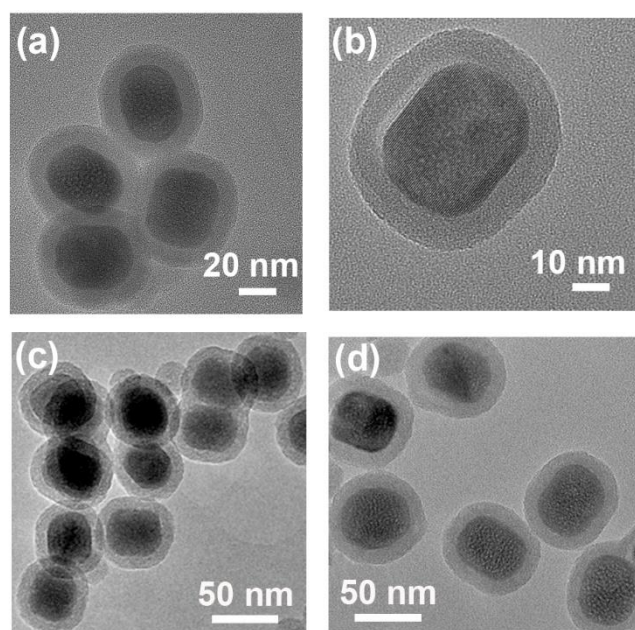

Fig. S1 Transmission electron microscopy (TEM) images of (a, b) UCNP@mSiO$_2$, (c, d) UCNP@mSiO$_2$@TDPM; 10 µL of the respective samples (1 mg/ 3 mL, ethanol) were drop-casted on the carbon-coated Cu grid.
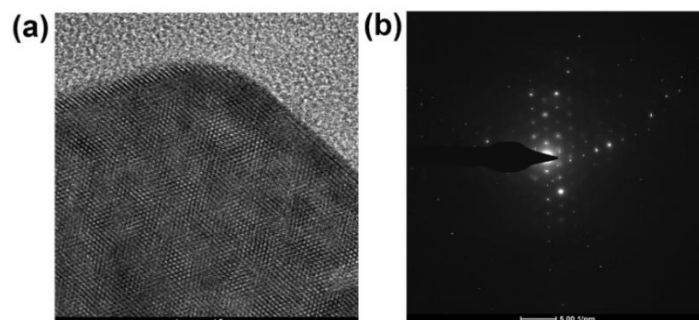

Fig. S2 (a) High-resolution transmission electron microscopy (HRTEM) image, and (b) selected area electron diffraction (SAED) pattern of UCNP.

3.2 Powder X-ray diffraction (PXRD)

The hexagonal phase of the UCNP was confirmed by the PXRD pattern, as shown in Fig. S3a (JCPDS no. 16-0334).[3] A new peak at $2\theta = 22°$ for UCNP@mSiO$_2$ suggested the successful coating of the amorphous silica on the surface of UCNP (Fig. S3b).[4]
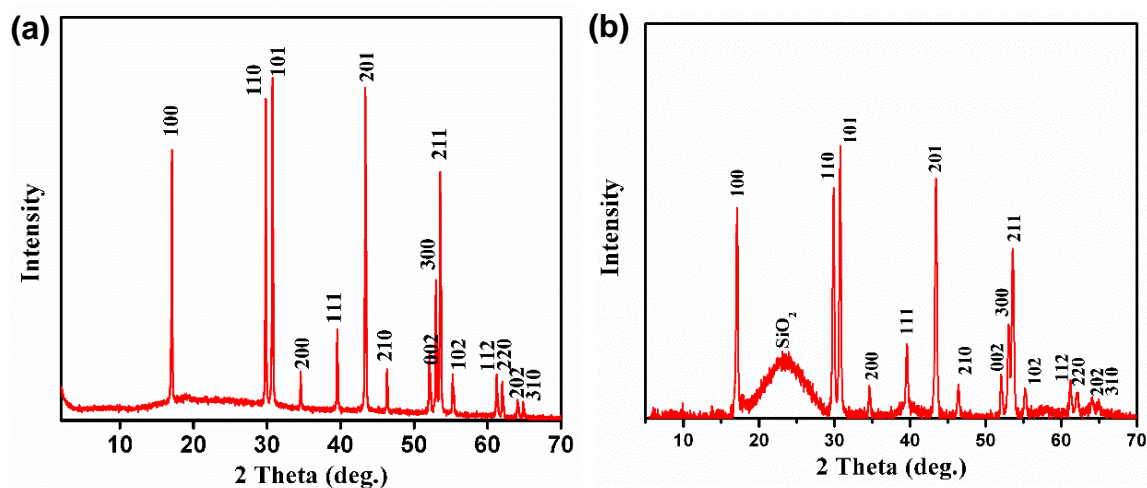

Fig. S3 Powder X-ray diffraction (PXRD) patterns of (a) UCNP, and (b) UCNP@mSiO$_2$.

3.3 Thermogravimetric analysis (TGA)

The samples were heated at a rate 10 °C min^{-1} under a nitrogen atmosphere up to 800 °C. The TGA plot showed the stability of UCNP and UCNP@mSiO$_2$ up to 330 °C (Fig. S4).[5]
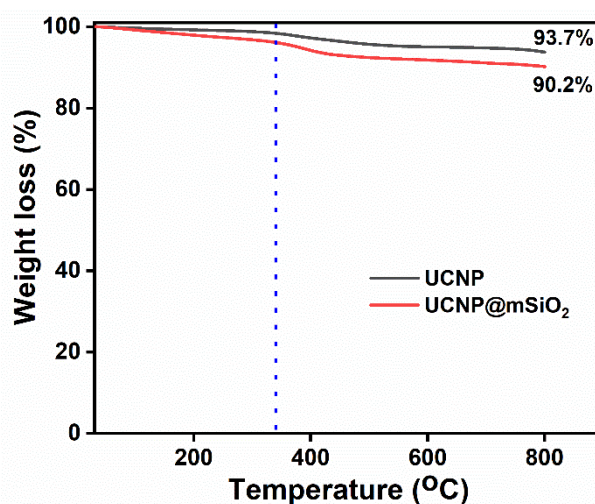

Fig. S4 Thermogravimetric analysis (TGA) curves of UCNP (black) and UCNP@mSiO$_2$ (red).

3.4 Brunauer-Emmett-Teller (BET) analysis

UCNP@mSiO$_2$ sample was dried for 24 h before the measurement. Then, the sample was degassed at 80 °C for 12 h under vacuum before analysis. Nitrogen adsorption/desorption isotherms were analyzed using ASiQwin software. Nitrogen sorption isotherms were measured at 77 K. The Brunauer-Emmett-Teller (BET) surface area of UCNP@mSiO$_2$ was found to be 74 m^2 g^{-1} with a total pore volume of 0.17 cm^3 g^{-1} at P/P$_0$ = 0.95 (Fig. S5a). The pore size was calculated using the nitrogen sorption isotherm employing the nonlocal density functional theory (NLDFT) method. The major contribution of pore widths was observed at 2.9 nm, along with the hierarchical distributions of mesopores (Fig. S5b).
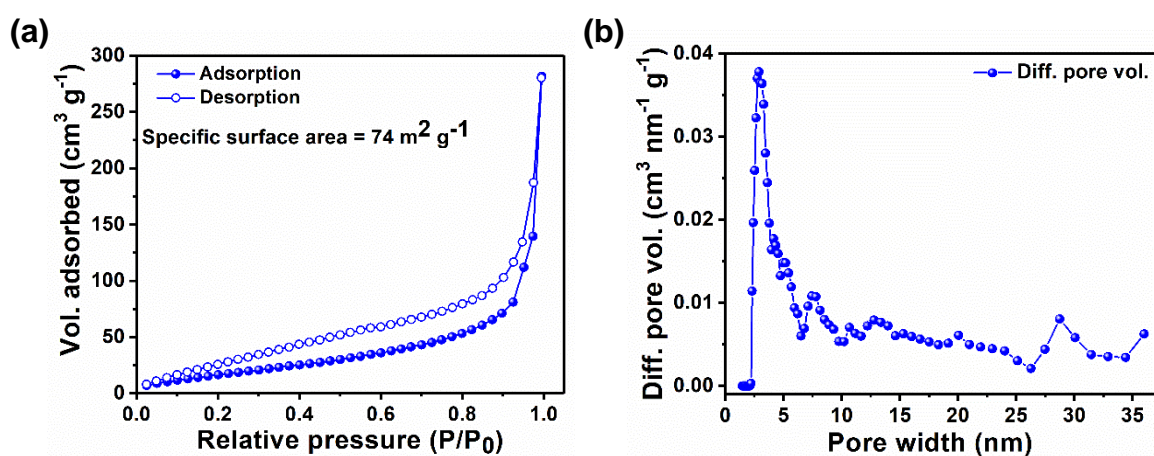

Fig. S5 (a) The nitrogen adsorption/desorption isotherms, and (b) pore size distribution of the UCNP@mSiO$_2$ nanoparticles obtained through the nonlocal density functional theory (NLDFT) method.

IV. Spectroscopic investigation

4.1 Absorption, emission, and excitation of TDPM

Normalized absorption, emission, and excitation spectra of TDPM (4 µM in DMSO) are shown in Fig. S6. Overlay of the excitation spectrum with that of the absorption spectrum signified that the emissions occurred from the same state to which the molecules were vertically excited.
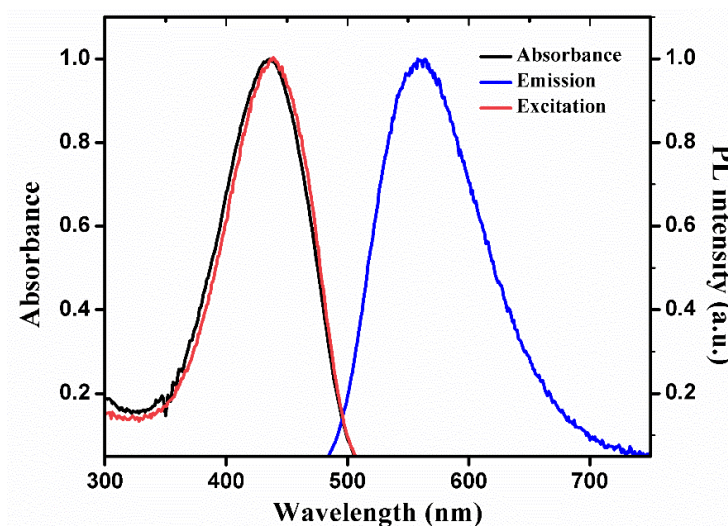

Fig. S6 Normalized absorption, emission (λ_{exc} = 440 nm), and excitation (λ_{em} = 570 nm) spectra of TDPM (4 µM in DMSO).

4.2 TDPM loading into UCNP@mSiO₂ matrix

In the typical dye loading procedure, 20 mg of UCNP@mSiO$_2$ was taken in a round bottom (RB) flask. Then, the TDPM solution (0.9 mM: 0.35 mg in 3 mL of DMSO) was added to obtain the hybrid upconversion nanoprobe (HN7). The reaction mixture was sonicated and kept for overnight stirring. The nanoprobe was centrifuged for 10 min at 6000 rpm. The final mixture was washed multiple times with DMSO and water. The absorbance of the supernatants
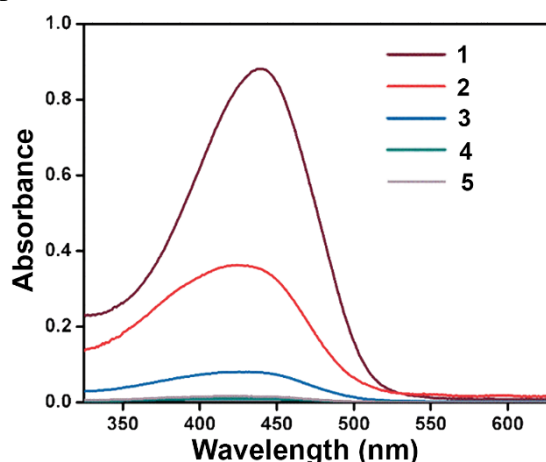

Fig. S7 Absorption spectra of the supernatant of hybrid upconversion nanoprobe dispersion after consecutive washing with DMSO for three times (1, 2, 3), and consecutive washing with water for two times (4, 5).

after each washing (DMSO and water) was monitored (Fig. S7). The spectrum 5 in Fig. S7 confirms the removal of the unloaded dye. Fig. S8 shows the comparative absorption profile of UCNP@mSiO$_2$, UCNP@mSiO$_2$@TDPM, and TDPM.
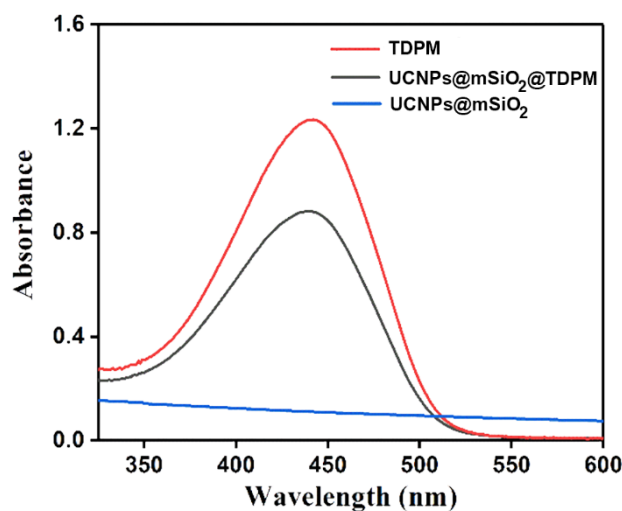

Fig. S8 Absorption spectra of TDPM, UCNP@mSiO$_2$@TDPM, and UCNP@mSiO$_2$ confirming the TDPM loading into the UCNP@mSiO$_2$ matrix.

4.3 Determination of the amount of TDPM loading into UCNP@mSiO$_2$ matrix for HN7

To determine the amount of TDPM loading, the absorption spectrum was recorded for the TDPM stock solution (0.35 mg in 3 mL of DMSO). The absorbance was saturated at an optical density (OD) 4. Therefore, the solution was diluted ten times, and then the absorption was recorded. From Beer Lambert's law, absorbance is directly proportional to the concentration of the probe.[6] Thus, the absorbance of the diluted solution was multiplied by 10 to estimate the absorbance (A$_1$) of the stock solution (Fig S9).
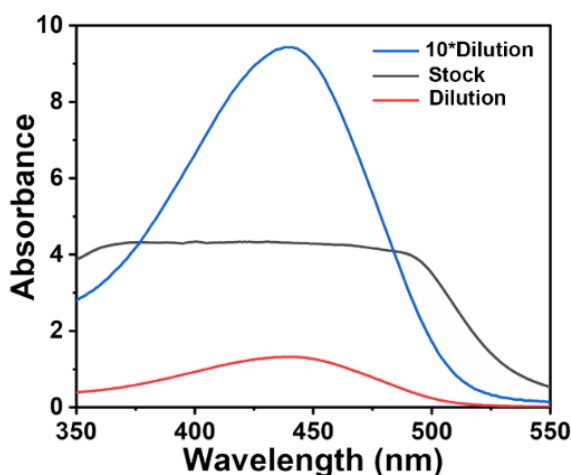

Fig. S9 Absorption spectra of TDPM (0.9 mM in DMSO).

The loading of TDPM in the nanoprobe was calculated using equations 1 and 2,

$$A = \epsilon.c.l \text{ -----------(1)}$$

where,

A = absorbance

ϵ = molar absorptivity

c = concentration of TDPM

l = path length

$$\frac{A_1}{A_2} = \frac{c_1}{c_2} \text{ --------------(2)}$$

A_1 is the absorbance of TDPM stock solution (Fig. S9),

A_2 is the absorbance of the hybrid upconversion nanoprobe (HN7; Fig. 4a) dispersion,

c_1 is the concentration of TDPM stock solution,

c_2 is the concentration of TDPM in hybrid upconversion nanoprobe (HN7),

$$\frac{9.4}{0.9} = \frac{0.35}{c_2}$$

$$c_2 = 33 \text{ µg}$$

Thus, 33 µg of TDPM was loaded in the hybrid upconversion nanoprobe (HN7).

4.4 Chemical transformation of TDPM to TDP-1

The optical properties of TDPM on the addition of hydrazine in DMSO was monitored (Fig. S10). A visual color change from yellow to colorless was noticeable, suggesting the chemical
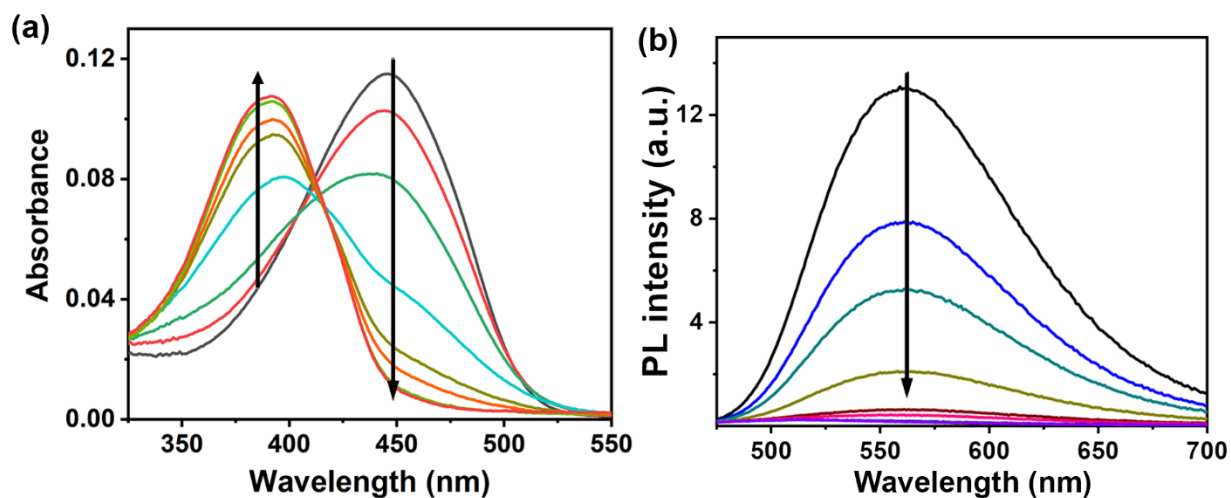

Fig. S10 (a) Absorption, and (b) emission (λ_{exc} = 445 nm) spectra of TDPM (4 µM) on addition of hydrazine in DMSO.

transformation from TDPM to TDP-1 (Fig. 1b, 1c, Scheme S3).[7-9] The significant change in absorption and emission was observed upon the addition of hydrazine to the TDPM solution (Fig. S10). The absorption peak of TDPM at 445 nm was gradually decreased, and a new peak at 390 nm was observed upon the successive addition of hydrazine (Fig. S10a). Similarly, the fluorescence intensity of TDPM at 570 nm was decreased upon the addition of hydrazine (Fig. S10b). The chemical transformation from TDPM to TDP-1 (corresponding hydrazone) upon the addition of hydrazine hydrate confirmed through MALDI analysis (Scheme S3, Fig. S11). The mass spectrum of TDP-1 showed peaks at m/z 324 corresponding to [M+4H$^+$]. Similar results were also observed upon treatment of TDPM with aliphatic biogenic amines like spermine (Fig. S12, S13).
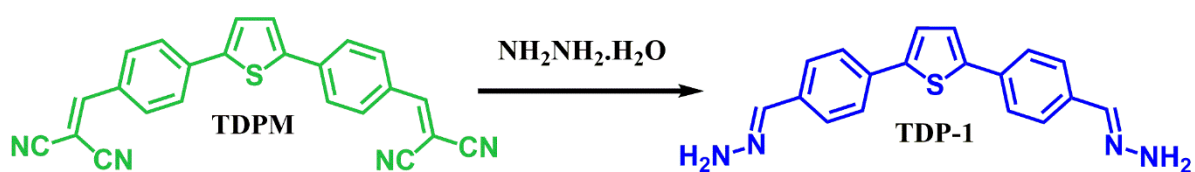
Scheme S3 Chemical transformation of TDPM to TDP-1 upon the addition of hydrazine hydrate.
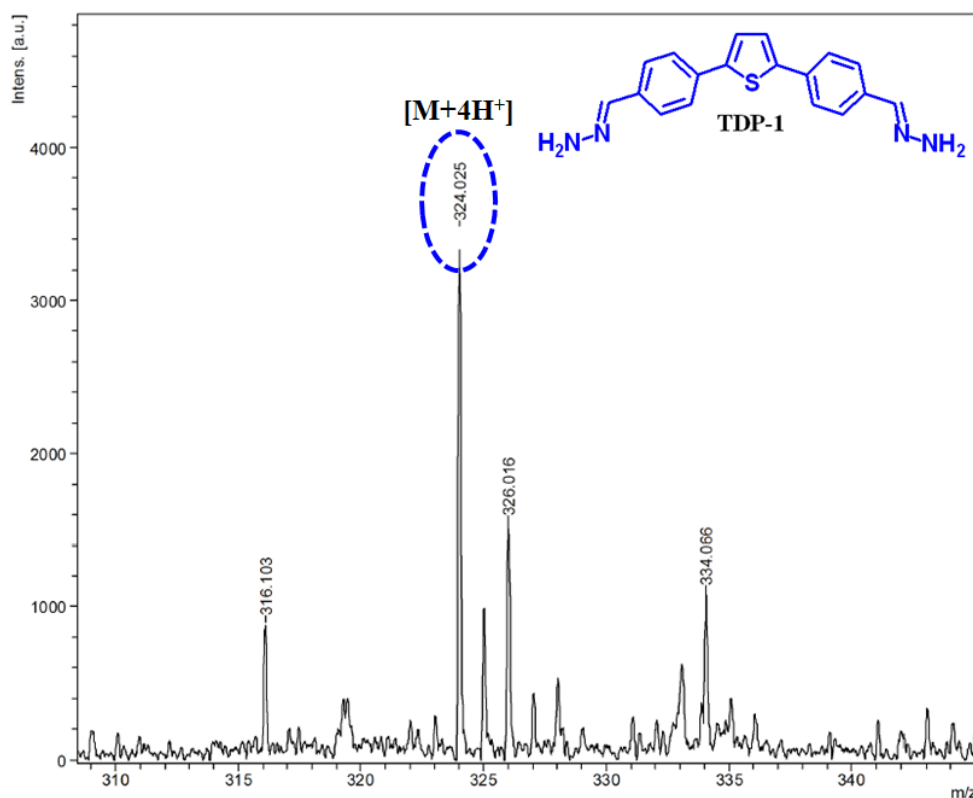
Mass data:

Fig. S11 MALDI data of the chemically transformed product (TDP-1) upon the addition of hydrazine hydrate to TDPM solution in dichloromethane.
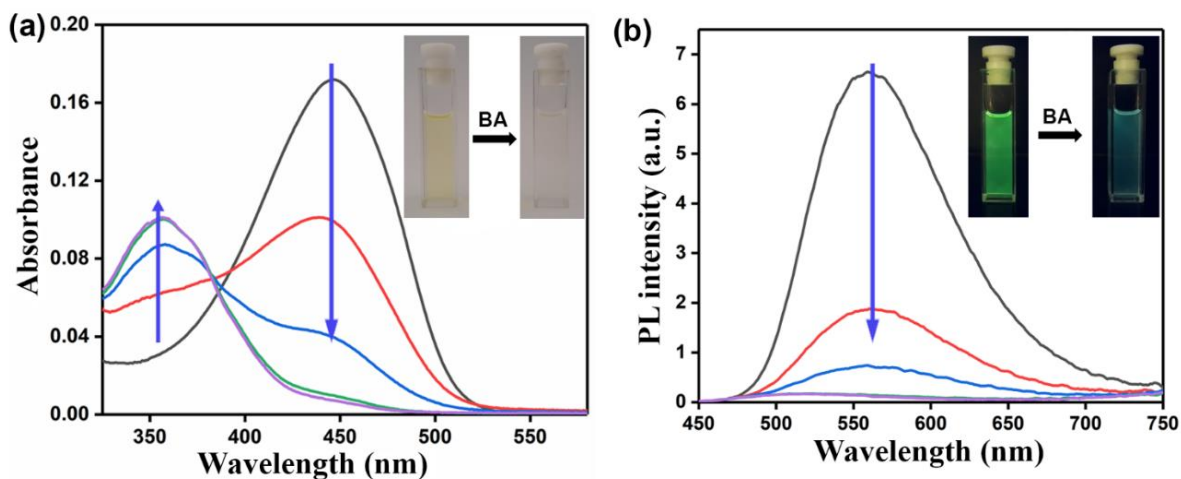
Fig. S12 (a) Absorption spectra of TDPM (4 µM) on the addition of spermine in DMSO; inset: the digital photographs of TDPM solution (DMSO) and the same solution upon addition of biogenic amine (BA, spermine) under visible light. (b) Emission spectra (λ_{exc} = 440 nm) of TDPM (4 µM) on the addition of spermine in DMSO; inset: the digital photographs of TDPM solution (DMSO) and the same solution upon addition of spermine under the illumination at 365 nm.
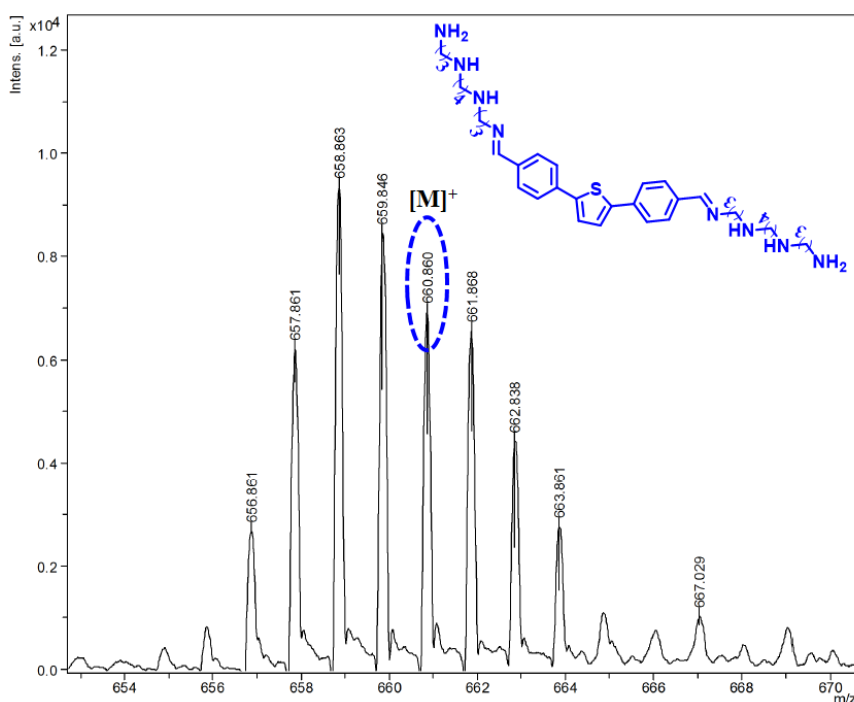
Mass data:

Fig. S13 MALDI data of the chemically transformed product (corresponding imine) upon the addition of spermine to TDPM solution in dichloromethane.

4.5 Unsuitability of TDPM for the detection of biogenic amines in an aqueous medium

Due to the insolubility of TDPM in water, it cannot be used for the detection of biogenic amines in an aqueous medium. To avoid the solubility issue, we measured the absorption and emission of TDPM in a binary solvent mixture (10% DMSO and 90% water, Fig. S14). A drastic reduction of fluorescence intensity of TDPM was noticeable upon the gradual increase of water percentage (Fig. S14b). Thus, TDPM could not be employed as a fluorescent sensor for biogenic amine in the aqueous medium. Further, the absorption spectra of TDPM were recorded in a mixture of 10% DMSO and 90% water with an excess of biogenic amine (Fig. S15a). The estimation of LOD was inconclusive due to a marginal change in absorption of TDPM even after the addition of biogenic amine at mM concentration level. (Fig. S15b). Hence, the systematic analyses unequivocally justified the superiority of the hybrid upconversion nanoprobe (UCNP@mSiO$_2$@TDPM) for the detection of aliphatic biogenic amines in the aqueous medium under lower energy NIR excitation over the pristine TDPM dye in the organic medium under higher energy excitation.
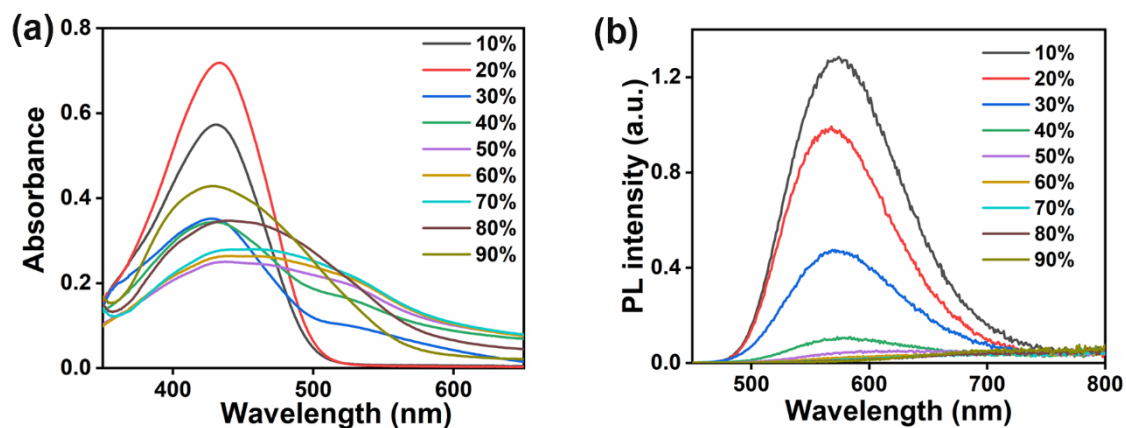

Fig. S14 (a) Absorption, and (b) emission spectra of TDPM ($\lambda_{exc} = 445$ nm, 10 μM) in a binary solvent mixture of DMSO and water with varying water fraction.
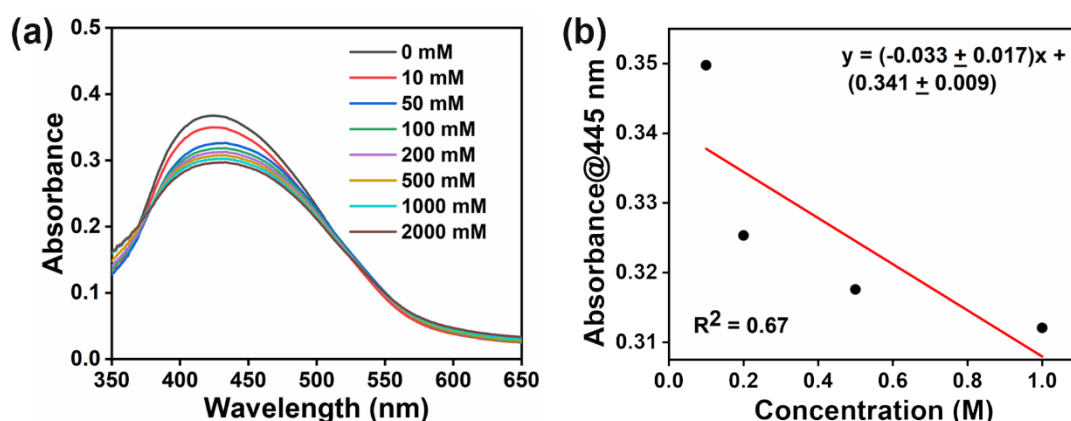

Fig. S15 (a) Absorption spectra of TDPM aggregates (10% DMSO-90% water) upon addition of spermine (0 − 2000 mM). (b) The absorbance of TDPM aggregates (10% DMSO-90% water) at 445 nm as a function of spermine concentration; the linear fitting of the data was not possible due to a minimal change in the absorption spectra even at higher spermine concentration.

4.6 Photoluminescence decay analysis

We carried out the decay analysis of the hybrid upconversion nanoprobes using a time-correlated single-photon counting (TCSPC) set up monitoring the UCNP (donor) emission at 475 nm. The energy transfer between UCNP and TDPM can be monitored through the decay analysis of Tm^{3+} emission at microsecond to millisecond timescale (typical for lanthanides) by the excitation at either 980 nm (absorption of Yb^{3+}) or 460-470 nm (direct ground state absorption of Tm^{3+}). Here, the decay analysis was carried out using 461 nm spectraLED (direct excitation of Tm^{3+}). We observed a decrease in the lifetime of Tm^{3+} (donor, λ_{em} = 475 nm) from 250 to 169 µs in hybrid upconversion nanoprobe upon the gradual increase of the TDPM loading (HN1 to HN7) compared to that of the pristine mesoporous silica-coated UCNP (Fig. S16). The results unambiguously ascertained the energy transfer from UCNP to TDPM rather than any reabsorption process. Moreover, the concomitant increase in the decay time for Tm^{3+} emission was observed upon the gradual addition of biogenic amine (spermine, 0.5 - 4.5 µM) to the dispersion of hybrid nanoprobe (HN7), indicating an inhibition of the energy transfer process. Similar decay profiles were noted in the literature reported earlier on upconversion nanoprobes delineating the resonance energy transfer from UCNP to a surface-bound fluorescent dye.[10] The results were also consistent with the general interpretation of RET process analysed through steady-state emission measurements.[11-14] A schematic illustration of simultaneous energy transfer from Yb^{3+} to Tm^{3+} and Tm^{3+} to TDPM is shown in Scheme S4.

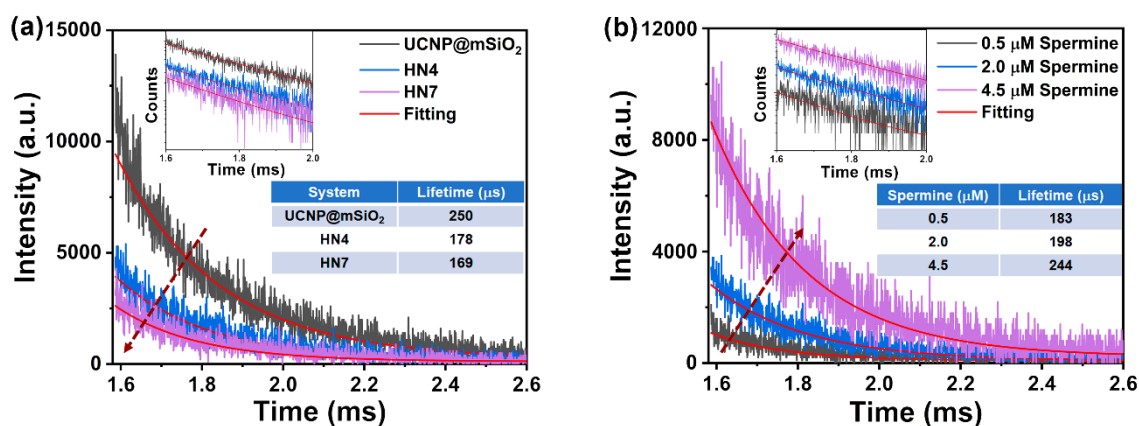**Fig. S16** Decay profiles (λ_{em} = 475 nm; λ_{ex} = 461 nm SpectraLED with FWHM = 23 nm) of (a) mesoporous silica-coated upconversion nanoparticle (UCNP@mSiO$_2$) and hybrid upconversion nanoprobe (UCNP@mSiO$_2$@TDPM, HN4, HN7) and (b) upon addition of spermine (0.5 to 4.5 µM) to HN7 aqueous dispersion (20 mg / 3 mL). Inset: the magnified decay profiles and the corresponding lifetime data in tabular format.
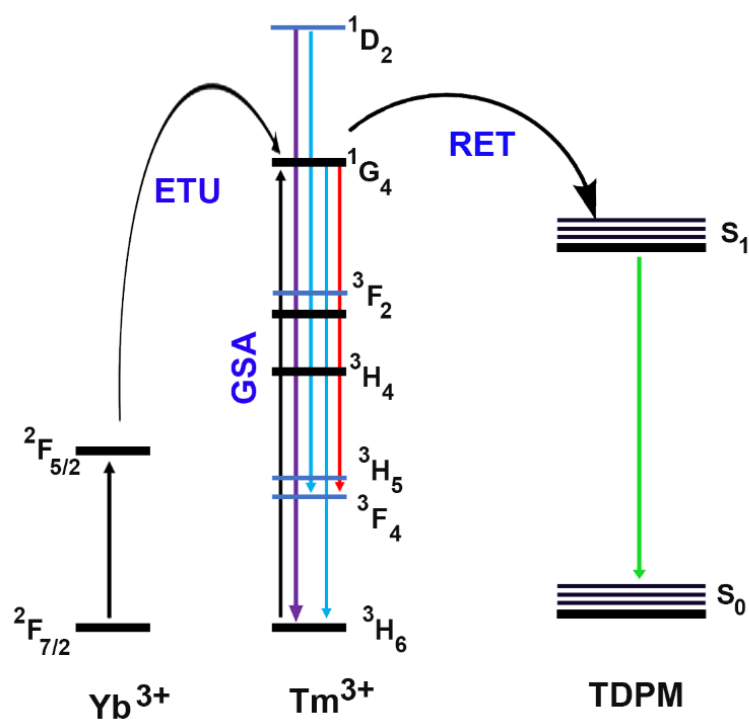
Scheme S4 Schematic illustration of energy level diagram depicting the energy transfer upconversion (ETU) from Yb^{3+} to Tm^{3+} and the resonance energy transfer (RET) from Tm^{3+} to TDPM. The ground state absorption (GSA) of Tm^{3+} is indicated.

4.7 The selectivity of the nanoprobe for different amines and ions

The selectivity of the hybrid upconversion nanoprobe was checked for various aliphatic biogenic amines, aromatic biogenic amines, representative diamines, and primary, secondary and tertiary amines (Table S1). The absorption and emission spectra of the hybrid upconversion nanoprobe were recorded. A significant change in the absorption and emission spectra of the nanoprobe was observed upon the addition of aliphatic biogenic amines like cadaverine, putrescine, and biogenic polyamines like spermine (Fig. 5c, main text, Fig. S17, S18). Both the electronic and the steric factors of amines governed the sensitivity of the hybrid upconversion nanoprobes. The higher nucleophilicity and less steric hindrance of aliphatic BAs in comparison to that of the aromatic counterpart might be the reason behind the observed sensing behavior (Table S1).[15]
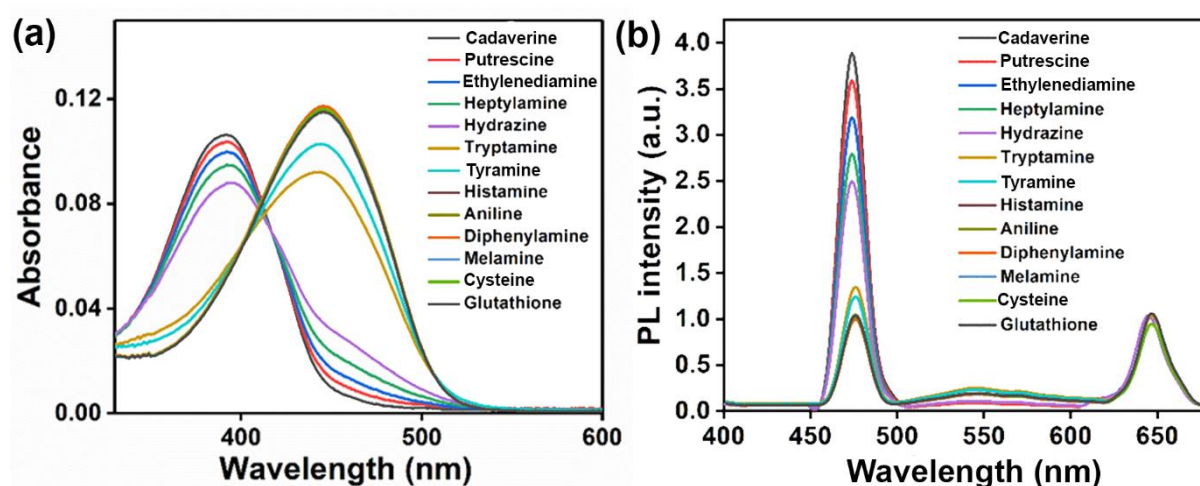

Fig. S17 (a) Absorption, and (b) emission spectra (λ_{exc} = 980 nm) of hybrid upconversion nanoprobe (20 mg / 3 mL water) in the presence of different amines (5 µM, water).
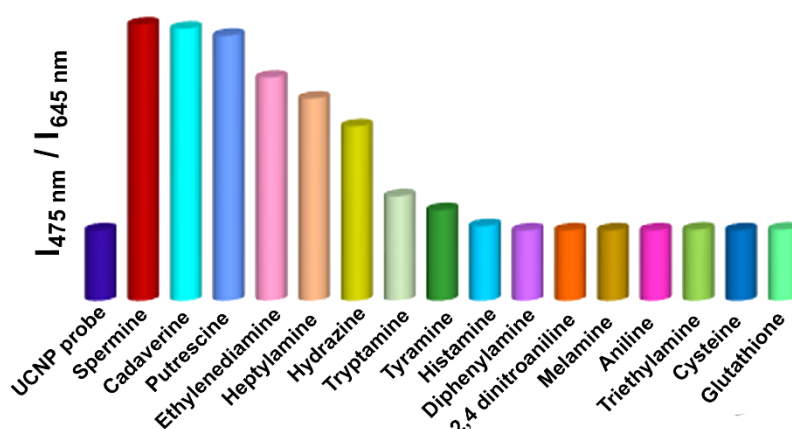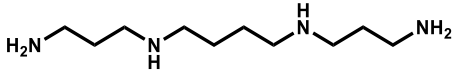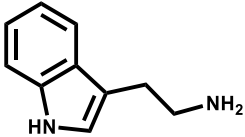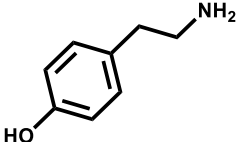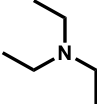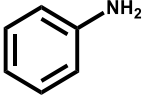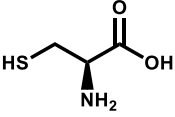

Fig. S18 Ratiometric photoluminescence responses (I_{475nm}/I_{645nm}, λ_{exc} = 980 nm) of UCNP@mSiO$_2$@TDPM aqueous dispersion (20 mg / 3 mL) upon the addition of diverse amines (5 µM, water).

Table S1: Molecular structure and pKa of conjugate acids of diverse amine, including aliphatic and aromatic biogenic amines employed for the sensing studies using hybrid upconversion nanoprobe.

Name	Structure	pKa (conjugate acid)	Sensitivity
Biogenic amines			
Spermine		11.1	High
Putrescine		10.51	High
Cadaverine		10.25	High
Hydrazine		8.10	Moderate
Tryptamine		9.73	Low
Tyramine		9.66	Low
Histamine		5.8, 9.4	No
Other amines			
Triethylamine		10.75	No
Aniline		4.6	No
Cysteine		Exist as a zwitterionic form	No

Glutathione		Exist as a zwitterionic form	No
2,4-Dinitroaniline		-4.53	No
Melamine		5.6	No
Diphenylamine		0.78	No
Ethylenediamine		9.69	Moderate
n-Heptylamine		10.67	Moderate

The optical response of the hybrid upconversion nanoprobe was also checked in the presence of various ions like Mn^{2+}, Zn^{2+}, Cd^{2+}, Ni^{2+}, Co^{2+}, Cu^{2+}, Al^{3+}, Fe^{3+}, NO_3^-, AcO^-, Cl^-, etc. The absorption and emission spectra were recorded for the nanoprobe upon addition of different ions under the excitation of 980 nm. However, no change was observed in the absorption as well as emission spectra for the hybrid upconversion nanoprobe in the presence of interfering ions (Fig. S19), making it promising for real-time detection of aliphatic biogenic amines during the food spoilage.
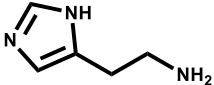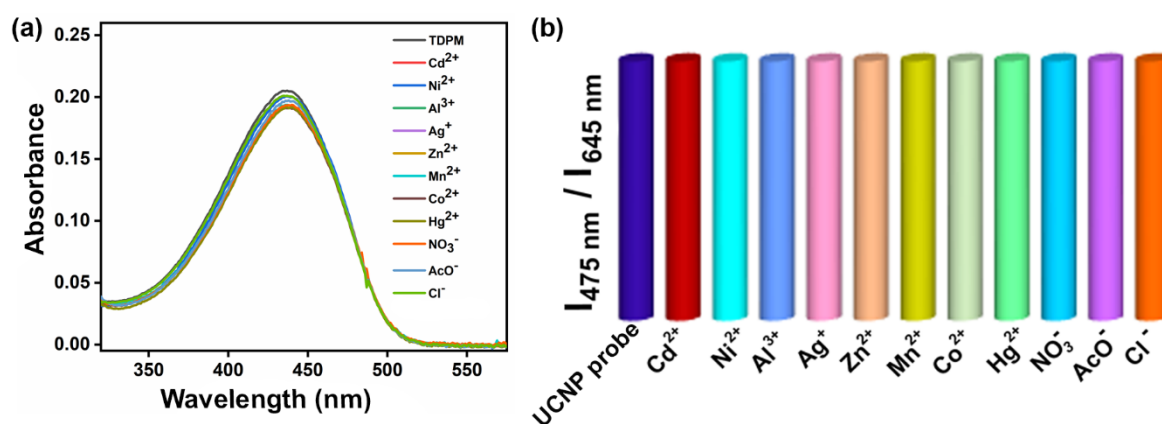

Fig. S19 (a) Absorption spectra, and (b) the ratiometric photoluminescence responses (I_{475nm} / I_{645nm}, $\lambda_{exc} = 980$ nm) of the hybrid nanoprobe (20 mg / 3 mL water) in the presence of different ions (5 μM, water).

4.8 Limit of detection of BAs using pristine hybrid upconversion nanoprobes

The ratiometric photoluminescence intensity of hybrid nanoprobe was plotted against aliphatic biogenic amines (spermine, cadaverine, and putrescine) concentration for the determination of limit of detection (LOD). The linear region of the resulting curve was fitted into a straight line (Fig. S20), and LOD was calculated according to the following equation.[16]

$$LOD = 3\sigma/k \text{----------(3)}$$

Where,

k = slope of the graph and σ = standard deviation of the intercept.

From Fig. S20, k = 0.265 µM, and σ = 0.0102. Thus,

LOD = 3 * 0.0102/0.265

LOD = 0.11 µM

The standard deviation in LOD of spermine was calculated through triplicate measurements and found to be (0.11 ± 0.02) µM.

Fig. S20 Ratiometric photoluminescence intensity of the hybrid upconversion nanoprobe in an aqueous dispersion as a function of spermine concentration and its linear fit. The bars represent the standard deviation through triplicate measurements.
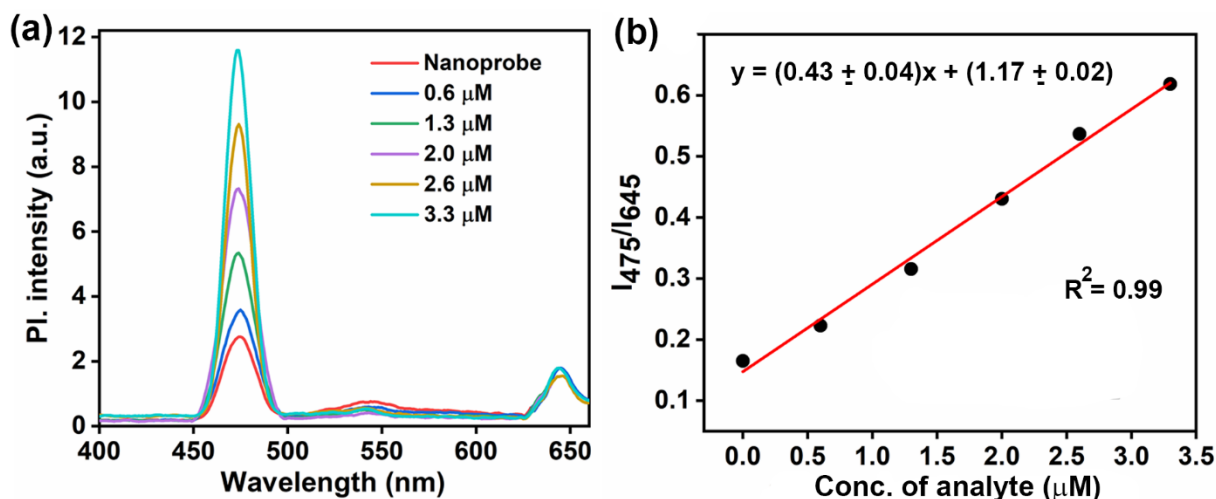
Fig. S21 (a) Emission spectra of the hybrid upconversion nanoprobe (20 mg / 3 mL water) with increasing concentration of cadaverine in the aqueous dispersion. (b) Ratiometric photoluminescence intensity of hybrid upconversion nanoprobe in an aqueous dispersion as a function of cadaverine concentration and its linear fit.

Fig. S22 (a) Emission spectra of the hybrid upconversion nanoprobe (20 mg / 3 mL water) with increasing concentration of putrescine in the aqueous dispersion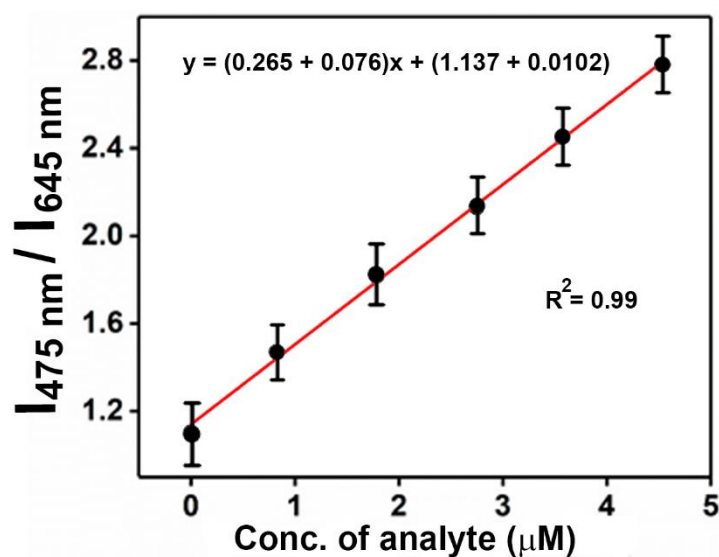. (b) Ratiometric photoluminescence intensity of hybrid upconversion nanoprobe in an aqueous dispersion as a function of putrescine concentration and its linear fit.

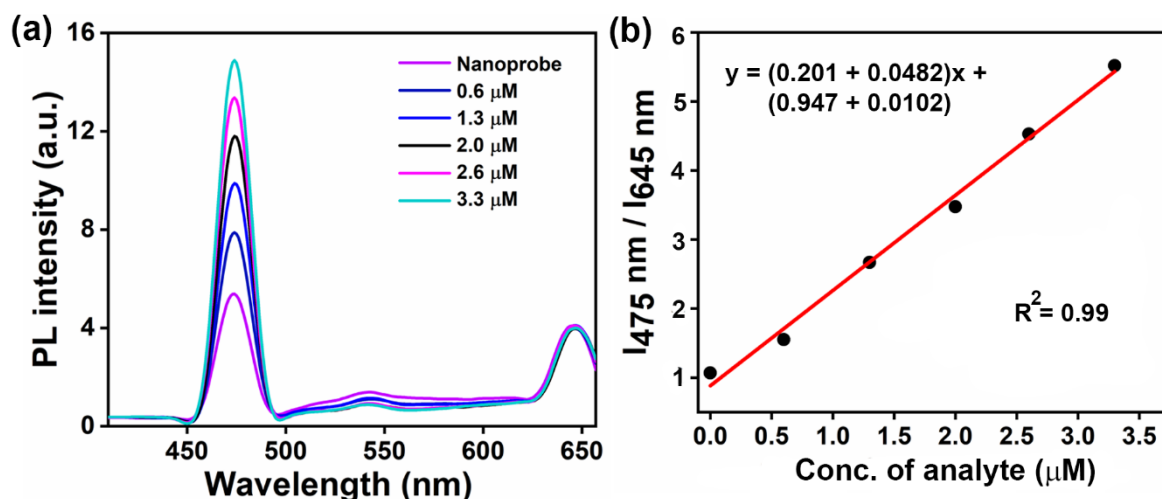The LODs for cadaverine and putrescine were also calculated in a similar way like spermine (Fig. S21, S22). The LODs for cadaverine and putrescine were found to be 0.13 and 0.15 μM, respectively.

V. Detection of aliphatic biogenic amine in milk

Milk was treated following a reported procedure.[17] 2 mL of 20% trichloroacetic acid in water was added to 10 mL of milk sample for protein coagulation. Afterward, the milk sample was centrifuged at 10,000 rpm for 30 min. The supernatant was then filtered through a 0.22 μm membrane to remove all the interfering substances in the milk. The upconversion luminescence intensity of the hybrid nanoprobe was recorded with the subsequent addition of the treated milk. No change in the emission spectra was observed with the varying amount of milk sample (Fig. S23). Furthermore, the milk sample was spiked with a varying concentration of spermine from 2.5 μM to 25 μM. Again, the experiment was repeated through the addition of spiked milk, and emission was recorded (Fig. 6a, main text). The recovery percentage and relative standard deviations are summarized in Table S2. The result suggests that the hybrid upconversion nanoprobe can detect the minimum concentration of 2.5 μM of spermine in adulterated milk samples, which is lower than the typical concentration of spermine found in cow milk.[18] The minimum concentrations of biogenic amines like cadaverine and spermine are found to be in the μM range in fresh dairy products [milk: cadaverine = 0.13 mg/kg (1.2 μM), spermine = 0.86 mg/kg (4.2 μM) and curd: cadaverine = 2.40 mg/kg (23.5 μM), spermine = 0.89 mg/kg (4.3 μM)].[18] Thus, the cut-off values of cadaverine and spermine can be considered as 1.2 μM and 4.2 μM, respectively, depicting the freshness of milk. Further, due to their prolonged storage at ambient conditions, the concentration of biogenic amines in such products is likely to be elevated due to decarboxylation in the presence of bacteria. The detection limit of spermine and cadaverine by the hybrid upconversion nanoprobe was 0.11 μM and 0.13 μM, respectively. Hence, the UCNP@SiO$_2$@TDPM probe can be used as a ratiometric sensor for monitoring the freshness of milk samples.
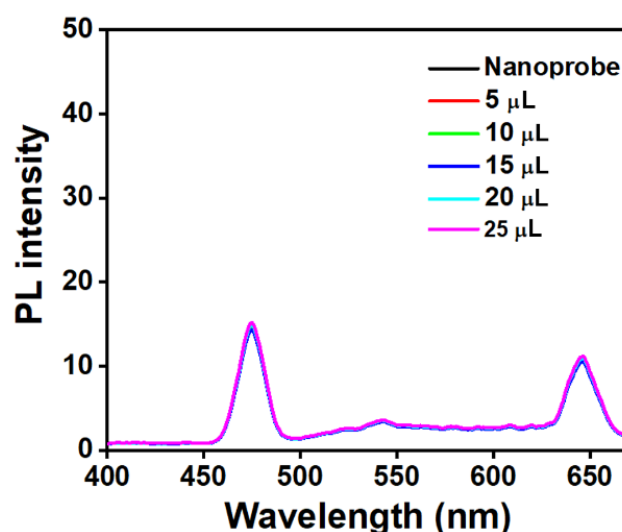
Fig. S23 Emission spectra of hybrid upconversion nanoprobe with an increasing amount of treated (unspiked) milk in an aqueous medium.

Table S2. The recovery percentage and relative standard deviation (RSD) of estimated biogenic amine (spermine) in pre-treated milk employing the hybrid upconversion nanoprobe.

Added (µM)	Found (µM)	Recovery (%)	RSD (%)
2.5	2.62 ± 0.08	104.8	3.2
5	5.10 ± 0.14	102.0	2.7
10	10.16 ± 0.28	101.6	2.8
15	15.05 ± 0.22	100.3	1.4
20	20.60 ± 0.80	103.0	3.5
25	25.80 ± 0.57	103.2	2.2

VI. Comparative analysis for the detection of different species using hybrid upconversion nanoprobe

Table S3: A comparative account on the detection of the biogenic amines through diverse kinds of materials (representative examples, including inorganic-organic composites, small organic molecules, and polymers) with hybrid upconversion nanoprobe developed in the present study.

Detecting probe	Absorption/ excitation wavelength (nm)	Emission wavelength (nm)	Detecting medium	Ratio-metric detection	Limit of detection	Application	References
Upconversion hybrid nanoprobe							
UCNPs@mSiO$_2$@TDPM	980	475, 645	Aqueous medium	Yes	0.11 µM (Spermine)	Detection in milk and fish	Present work (*first report*)
Inorganic-organic materials							
CdSe/ZnS quantum dots with graphene	400	610	Aqueous medium	No	0.021 mg L^{-1} (Tyramine)	Detection in rice	*Anal. Methods*, 2018, **10**, 3884.[19]
CdTe quantum dots-coated amphiphilic thiophene copolymers	425	500	Aqueous medium	No	2.90 nmol L^{-1} (Spermine)	-	*Sens. Actuators B Chem.*, 2018, **257**, 734.[20]
Cd-BBI metal organic framework (BBI = bisimidazole tetraacid)	370	450	Organic medium (Ethanol)	No	56 ppb (Spermine)	-	*J. Mater. Chem. C*, 2020, **8**, 11449.[15]
Small organic molecules							
Benzoannulated perylenediimide	440	478, 580	Organic medium (Chloroform)	Yes	180 pM	Detection in raw fish	*ACS Appl. Mater. Interfaces*, 2019, **11**, 47207.[21]
Naphthalene diimides	520	-	Aqueous medium	No	-	-	*Org. Chem. Front.*, 2018, **5**, 2641.[22]
*N, N-*dimethylaminonaphthalene anhydride	385	448, 578	Organic medium (Dimethylacetamide)	Yes	17 nM (Phenethylamine)	-	*Analyst*, 2016, **141**, 827.[23]
Arylalkylamine *N*-acetyltransferase	412	-	-	No	5 µM (Histamine)	Detection in milk and wine	*Chem. Commun.*, 2015, **51**, 8712.[17]

Polymers							
Nitrated polythiophene based polymer	450	-	Vapour phase detection	No	0.45 ppm (Putrescine)	-	_Sens. Actuators B. Chem.,_ 2018, **271**, 183.[24]
Carboxylated polyfluorene (PFTBTCOOH)	389	615, 696	Organic medium (THF)	Yes	10 μM (Spermine)	Detection in milk and yogurt	_ACS Appl. Mater. Interfaces,_ 2017, **9**, 22875.[25]
Poly[9,9-bis(6'-bromohexyl) fluoreneco-4,7-(2,1,3-benzothiadiazole)	350	415, 545	Aqueous medium	Yes	0.33 μM (Spermine)	Detection in urine	_Anal. Chem.,_ 2016, **88**, 7358.[26]
2,4,6-Trinitrobenzene based polymer	440	-	Organic medium (Acetone)	No	-	Detection in meat and fish	_Chem. Eur. J.,_ 2015, **21**, 8733.[27]

Table S4: A comparative account on diverse kinds of hybrid upconversion nanoprobes employed for sensing with the nanomaterial developed in the present study.

Composite materials		Analytes	Ratiometric detection	Limit of detection	References
UCNPs	Receptor unit				
UCNPs@mSiO$_2$@TDPM UCNPs =NaYF$_4$, Yb^{3+}, Tm^{3+}	Thiophene based molecule (TDPM)	Aliphatic biogenic amines	Yes	0.11 μM	Present work
Amines and amino acids					
CD-UCNPs UCNPs = NaYF$_4$, Yb^{3+}, Er^{3+} CD = α-cyclodextrin	Ring-opened rhodamine	Cysteine	No	1.1 μM	*Chem. Commun.,* 2015, **51**, 14054.[28]
UCNPs@mSiO$_2$ UCNPs = NaLuF$_4$, Yb^{3+}, Er^{3+}, Tm^{3+}	Iridium (III) complex	Cysteine/ Homocysteine	Yes	Cysteine = 28.5 μM	*ACS Appl. Mater. Interfaces,* 2014, **6**, 11190.[29]
DNB capped NaYF$_4$, Er^{3+}, Yb^{3+}	3,5-dinitrobenzoic acid (DNB)	Melamine	No	2.5 nM	*ACS Appl. Mater. Interfaces,* 2014, **6**, 7833.[10]
Biologically relevant small molecules					
PAAO-UCNPs-DCM-H$_2$O$_2$ UCNPs = NaYF$_4$, Yb^{3+}, Er^{3+}, Nd^{3+}@NaYF$_4$, Nd^{3+}	Dicyanomethylene- 4H-pyran (DCM)− H$_2$O$_2$	Hydrogen peroxide (H$_2$O$_2$)	Yes	0.168 μM	*ACS Appl. Mater. Interfaces,* 2019, **11**, 7441.[14]
PAAO-UCNPs-RhBs UCNPs = NaYF4, Yb^{3+}, Er^{3+}, Nd^{3+}@NaYF$_4$, Nd^{3+}	Rhodamine B	Nitric oxide (NO)	Yes	0.21 μM	*Nanoscale,* 2018, **10**, 10641.[13]
TPAMC-UCNPs@PEG. UCNPs = NaYF$_4$, Yb^{3+}, Er^{3+}, Tm^{3+}	Merocyanine triphenylamine-merocyanine (TPAMC)	Hydrogen sulfide (H$_2$S)	Yes	0.22 μM	*ACS Appl. Mater. Interfaces,* 2018, **10**, 39544.[30]
UCNP-MSN-*β*-CD UCNPs = NaYF$_4$, Er^{3+}, Yb^{3+}	Rhodamine B	Nitric oxide (NO)	Yes	73 nM	*J. Am. Chem. Soc.,* 2017, **139**, 12354.[12]
Ion sensing					
PEG-UCNPs UCNPs = NaYF$_4$, Yb^{3+}, Er^{3+}, Tm^{3+}	Cyanine dye CYDAC16	Cu^{2+}	Yes	37 nmol/L	*ACS Appl. Mater. Interfaces,* 2019, **11**, 430.[31]
UCNPs@SiO$_2$ UCNPs = NaYF$_4$, Yb^{3+}, Er^{3+}, Tm^{3+}	RB-FC	Cu^{2+}	Yes	0.11 μM	*ACS Appl. Mater. Interfaces,* 2018, **10**, 1028.[32]

CD-UCNPs UCNPs = $NaYF_4$, Yb^{3+} /Er^{3+} CD = α-cyclodextrin	Thiazole-derivative	Hg^{2+}	No	0.063 μM	*Nanoscale*, 2016, **8**, 276.[33]
UCNPs@$mSiO_2$ UCNPs = $NaYF_4$, Yb^{3+}, Er^{3+}, Tm^{3+}	Merocyanine-based dye	HS^-	Yes	0.58 μM	*ACS Appl. Mater. Interfaces,* 2014, **6**, 11013.[34]
CD-UCNPs UCNPs = $NaYF_4$, Yb^{3+}, Ho^{3+} CD = cyclodextrin	Rhodamine B derivative	Fe^{3+}	Yes	1.2 μM	*Chem. Commun.,* 2013, **49**, 7797.[35]

VII. References

1. K. Guo, F. Zhang, S. Guo, K. Li, X. Lu, J. Li, H. Wang, J. Cheng and Q. Zhao, *Chem. Commun.*, 2017, **53**, 1309.

2. K. Guo, H. Wang, J. Cheng, Y. Miao and J. Yang, 2014, CN 103788682 A 20140514.

3. T. Ma, Y. Ma, S. Liu, L. Zhang, T. Yang, H. Yang, W. Lv, Q. Yu, W. Xu, Q. Zhao and W. Huang, *J. Mater. Chem. C*, 2015, **3**, 6616.

4. R. Han, J. Shi, Z. Liu, Y. Hou and Y. Wang, *ACS Biomater. Sci. Eng.,* 2018, **4**, 3478.

5. A. Sedlmeier and H. H. Gorris, *Chem. Soc. Rev.*, 2015, **44**, 1526.

6. J. R. Lakowicz, *Principles of fluorescence spectroscopy*, Springer, New York, 2006.

7. M. Sun, J. Guo, Q. Yang, N. Xiao and Y. Li, *J. Mater. Chem. B*, 2014, **2**, 1846.

8. X. Yang, Y. Liu, Y. Wu, X. Ren, D. Zhang and Y. Ye, *Sens. Actuators B Chem.*, 2017, **253**, 488.

9. B. Roy and S. Bandyopadhyay, *Anal. Methods*, 2018, **10**, 1117.

10. C. Hazra, V. N. K. B. Adusumalli and V. Mahalingam, *ACS Appl. Mater. Interfaces*, 2014, **6**, 7833.

11. J. Peng, W. Xu, C. L. Teoh, S. Han, B. Kim, A. Samanta, J. C. Er, L. Wang, L. Yuan, X. Liu and Y. Chang, *J. Am. Chem. Soc.,* 2015, **137**, 2336.

12. N. Wang, X. Yu, K. Zhang, C. A. Mirkin and J. Li, *J. Am. Chem. Soc.*, 2017, **139**, 12354.

13. H. Wang, Y. Liu, Z. Wang, M. Yanga and Y. Gu, *Nanoscale*, 2018, **10**, 10641.

14. H. Wang, Y. Li, M. Yang, P. Wang and Y. Gu, *ACS Appl. Mater. Interfaces*, 2019, **11**, 7441.

15. S. Jindal, V. K. Maka and J. N. Moorthy, *J. Mater. Chem. C*, 2020, **8**, 11449.

16. A. Deshmukh, S. Bandyopadhyay, A. James and A. Patra, *J. Mater. Chem. C*, 2016, **4**, 4427.

17. P. Leng, F. Zhao, B. Yin and B. Ye, *Chem. Commun.*, 2015, **51**, 8712.

18. D. M. Linares, M. C. Martin, V. Ladero, M. A. Alvarez and M. Fernandez, *Food Sci. Nutr.*, 2011, **51**, 691.

19. Q. Wang and D. Zhang, *Anal. Methods*, 2018, **10**, 3884.

20. S. M. Tawfik, J. Shim, D. B. Speziale, M. Sharipov and Y. Lee, *Sens. Actuators B Chem.*, 2018, **257**, 734.

21. R. Roy, N. R. Sajeev, V. Sharma and A. L. Koner, *ACS Appl. Mater. Interfaces,* 2019, **11**, 47207.

22. A. Weißenstein, V. Grande, C. R. Saha-Möller and F. Würthner, *Org. Chem. Front.,* 2018, **5**, 2641.

23. S. Mallick, F. Chandra and A. L. Koner, *Analyst*, 2016, **141**, 827.

24. Y. Jin and G. Kwak, *Sens. Actuators B. Chem.*, 2018, **271**, 183.

25. H. Zhong, C. Liu, W. Ge, R. Sun, F. Huang and X. Wang, *ACS Appl. Mater. Interfaces*, 2017, **9**, 22875.

26. A. H. Malik, S. Hussain and P. K. Iyer, *Anal. Chem.*, 2016, **88**, 7358.

27. J. L. Pablos, S. Vallejos, A. Muńoz, M. J. Rojo, F. Serna, F. C. Garcìa and J. M. Garcìa, *Chem. Eur. J.*, 2015, **21**, 8733.

28. J. Ni, C. Shan, B. Li, L. Zhang, H. Ma, Y. Luo and H. Song, *Chem. Commun.*, 2015, **51**, 14054.

29. L. Zhao, J. Peng, M. Chen, Y. Liu, L. Yao, W. Feng and F. Li, *ACS Appl. Mater. Interfaces*, 2014, **6**, 11190.

30. X. Li, H. Zhao, Y. Ji, C. Yin, J. Li, Z. Yang, Y. Tang, Q. Zhang, Q. Fan and W. Huang, *ACS Appl. Mater. Interfaces,* 2018, **10**, 39544.

31. Y. Shi, Q. Liu, W. Yuan, M. Xu, W. Feng and F. Li*, ACS Appl. Mater. Interfaces,* 2019, **11**, 430.

32. B. Gu, M. Ye, L. Nie, Y. Fang, Z. Wang, X. Zhang, H. Zhang, Y. Zhou and Q. Zhang, *ACS Appl. Mater. Interfaces*, 2018, **10**, 1028.

33. B. Gu, Y. Zhou, X. Zhang, X. Liu, Y. Zhang, R. Marks, H. Zhang, X. Liu and Q. Zhang, *Nanoscale*, 2016, **8**, 276.

34. S. Liu, L. Zhang, T. Yang, H. Yang, K. Y. Zhang, X. Zhao, W. Lv, Q. Yu, X. Zhang, Q. Zhao, X. Liu and W. Huang, *ACS Appl. Mater. Interfaces*, 2014, **6**, 11013.

35. Y. Ding, H. Zhu, X. Zhang, J. Zhu and C. Burda, *Chem. Commun.,* 2013, **49**, 7797.

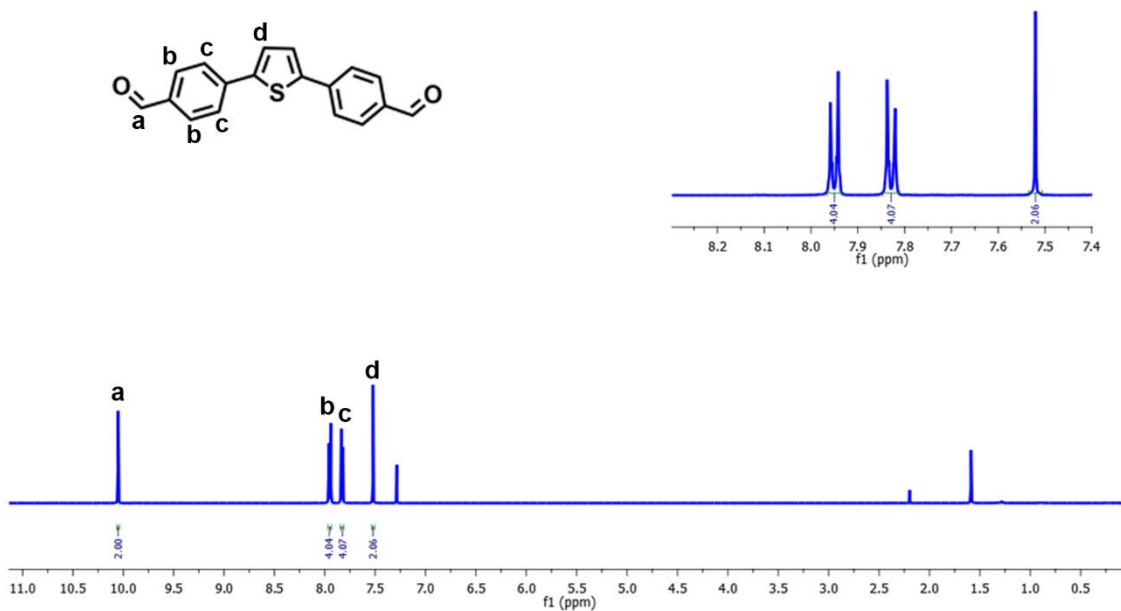# VIII. ^{1}H NMR spectra

8.1 ^{1}H NMR spectrum of TBA

Fig. S24 ^{1}H NMR spectrum of TBA in CDCl$_3$ at room temperature.
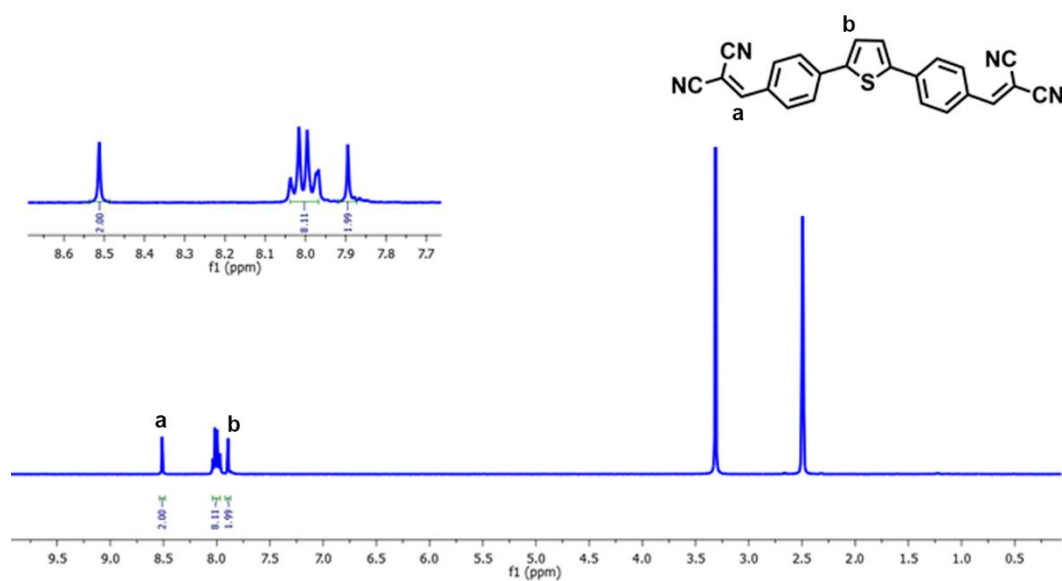
8.2 ^{1}H NMR spectrum of TDPM

Fig. S25 ^{1}H NMR spectrum of TDPM in DMSO-d$_6$ at room temperature.